ELSEVIER

PII: S0032-3861(96)01001-4

Polymer Vol. 38 No. 16, pp. 4165–4173, 1997

0032-3861/97/$17.00+0.00

Amorphous phase orientation in biaxially drawn poly(ethylene terephthalate) films

J. B. Faisant de Champchesnel and J. F. Tassin*
Université du Maine, Laboratoire de Physicochimie Macromoléculaire, URA CNRS no. 509, Avenue Olivier Messiaen, BP535, 72017 Le Mans Cedex, France

and L. Monnerie and P. Sergot
Ecole Supérieure de Physique et Chimie de Paris, Laboratoire de Physicochimie Structurale et Macromoléculaire, URA CNRS no. 278, 10, Rue Vauquelin, 75231 Paris Cedex 05, France

and G. Lorentz
Rhône-Poulenc Films, Magphane International, Saint Maurice de Beynost, BP140, 01701 Miribel Cedex, France
(Received 31 July 1996)

An experimental study of the development of molecular orientation in the amorphous phase during the transverse drawing of one-way drawn poly(ethylene terephthalate) films has been carried out. Both the behaviours of phenyl ring normals or chain axes and of fluorescent rigid probes have been considered. The influence of the size of the crystallites in the one-way drawn films has been studied. It is first shown that the phenyl ring normals in the amorphous phase tend to become more perpendicular to the draw direction, as expected. However, there is no marked tendency for the rings to lie in the plane of the film, on the contrary with the crystalline phase. The chain axes, as well as the fluorescent probes, tend to align along the second draw direction. In films possessing initially long crystals, this reorientation appears less efficient at equivalent draw ratios. A memory of the state of the amorphous orientation in the one-way drawn films is observed in the sense that more relaxed one-way drawn films will lead to broader distributions in the final biaxially stretched films. © 1997 Science Ltd.

(Keywords: poly(ethylene terephthalate); drawn films; orientation)

INTRODUCTION

Improvement of the mechanical properties and quality of sequentially biaxially stretched poly(ethylene terephthalate) (PET) films requires the knowledge at a molecular scale of the chain deformation processes and of the development of structure involved during the industrial process.

Previous studies in our group have dealt with the influence of the macroscopic parameters (temperature, strain rate, draw ratio), analysed through spectroscopic techniques, on the uniaxial planar drawing process[1–7]. The setting up of a specially designed stretching machine has allowed us to study the main processes involved in the transverse drawing under well defined conditions[8]. It is known from film manufacturers that the film drawability during the second step is highly dependent on the structure of the initial one-way drawn film. The influence of the monodrawn film's structure on the development of the morphology and orientation of the crystalline phase has been previously reported[9]. The present paper is devoted to the characterization of the molecular orientation in the amorphous phase and its behaviour throughout the transverse drawing process. In this context, the influence of the state of the monodrawn films will also be discussed, as in ref. 9.

Various methods have been proposed to obtain information about amorphous phase orientation. The most widely used is based on the fact that refractive indices or infra-red (i.r.) dichroism measurements yield information about orientation averaged over both the crystalline and amorphous phase. Assuming a two-phase model, amorphous orientation can be calculated if crystalline orientation has been independently measured using X-ray diffraction[10]. The same idea has been applied to average orientation data obtained by sonic modulus[11,12] measurements. Direct information on the amorphous phase orientation can be obtained using modern solid-state nuclear magnetic resonance techniques[13,14] or fluorescence polarization. Measurements of polarized fluorescence intensities have been used to characterize the orientation of rigid fluorescent probes located in the amorphous phase[15] and, more recently, the chain-intrinsic fluorescence of PET[16–18] has also been considered.

In this study, a combination of X-ray with birefringence or i.r. dichroism data will be used to obtain information about the orientation in the amorphous phase, and the results will be compared with a direct measurement of the orientation of rod-like molecules using fluorescence polarization. The influence of the

* To whom correspondence should be addressed

state of the one-way drawn films on amorphous phase orientation will be discussed.

MATERIALS

In order to carry out fluorescence polarization measurements, a fluorescent dye 4,4′-dibenzoxazolylstilbene (VPBO) has been incorporated into the polymer during the polycondensation reaction at a weight fraction of 100 ppm. The weight average molecular weight of the polymer is 39 000 g mol^{-1} and a glass transition temperature of 80°C has been measured, for an amorphous sample, by differential scanning calorimetry at a heating rate of 20°C min^{-1}.

The one-way drawn samples have been produced in a pilot plant which allows us to control the draw ratio and the stretching temperature, estimated from the film surface using an i.r. camera. Besides these parameters, the state of the monodrawn film can also be modified by the type of drawing[19,20]. Films can be either stretched 'at equilibrium' or 'quenched', depending on whether the sample has reached the equilibrium deformation under the applied conditions of load and temperature or the deformation process has been stopped before reaching this equilibrium state.

In the present study, one-way drawn samples are either 'at equilibrium', and in this case contain large crystals, or 'quenched' possessing thereby smaller ones. The present samples are included in the set of films, the crystalline structure of which has been characterized in detail in ref. 9. Some of the characteristics (draw temperature, draw ratio, crystallinity) of the monodrawn films are reported in *Table 1*.

Transverse stretching of the one-way drawn samples

For the second draw, samples were cut from the one-way drawn samples and stretched transversally to the first drawing direction on a specially designed drawing machine at the Saint Fons Research Centre of Rhône Poulenc[8]. The width normal to the second draw direction was kept constant at 100 mm. The samples were stretched, as described in ref. 9, at a stretching temperature of 120°C. In order to bring the sample from ambient to the stretching temperature, T_2, the following preheating programme was applied to each sample prior to stretching: 30 s heating at 87°C followed by 3 s heating at the second drawing temperature. Transverse stretching, with maximum draw ratios up to $\lambda = 4$, was conducted at an initial strain rate of 0.25 s^{-1}. The effective draw ratio was measured by means of a grid placed on the samples and only the central portion of the specimen was considered for further characterization. In the sample notation, the letter (s) or (l) is used to characterize one-way drawn films having either short or long crystals, respectively. The first number indicates the longitudinal drawing temperature and the second one the corresponding draw ratio. If more numbers are used, the same indications about the second (transverse) drawing are added.

Table 1 Characteristics of one-way drawn films

Kind of sample	First drawing temperature T_1 (°C)	First draw ratio (λ_1)	Crystallinity (%)
	100	3.2	8.6
Quenched:	100	3.3	9.9
small	103	3.4	8.6
crystallites	105	3.2	7.2
	105	3.5	9.7
Plateau:	100	3.9	25.2
large	105	3.6	29.5
crystallites	125	3.4	28.0

GENERAL THEORETICAL BACKGROUND

Description of orientation in space (3D)

Spectroscopic techniques give access to the second and eventually the fourth order moments of the distribution function of a molecular direction i with respect to the principal macroscopic directions J of the sample. Those moments can be written either in terms of the average cosinus $\langle \cos^n \theta_{i/J} \rangle$ or of the average values $P_{n00}^{i/J}$ of the second order Legendre polynomial $P_n(\cos\theta)$, defined as[15]

$$P_{200}^{i/J} = \tfrac{1}{2}\langle 3\cos^2\theta_{i/J} - 1\rangle \quad (1)$$

$$P_{400}^{i/J} = \tfrac{1}{8}\langle 35\cos^4\theta_{i/J} - 30\cos^2\theta_{i/J} + 3\rangle \quad (2)$$

where $\theta_{i/J}$ is the angle between the molecular direction i and the macroscopic direction J, and the brackets denote an average over all molecular units.

P_{200} takes a value of 0 when the distribution of units is isotropic, and 1 when all the units are aligned parallel to the reference axis with respect to which P_{200} is calculated. From those $\langle \cos^n \theta_{i/J} \rangle$ (or P_{200}) values, it is possible to create a most probable distribution function (MPDF)[21,22]; the higher the order of the $\langle \cos^n \theta_{i/J} \rangle$ (or P_{n00}), the more realistic the shape of the MPDF. Bower[21,22] showed that, in the case of polymers, the MPDF gives a very realistic shape when moments up to the fourth order are taken into account.

Distribution in a plane (2D)

In the special case where the direction i of all units is confined in a plane, e.g. the plane of the film, some simplifications occur. Let us call X_1 and X_2 the two principal directions of the plane, and X_3 the direction normal to the plane. We then have

$$\langle \cos^2\theta_{i/3} \rangle = 0 \quad (3)$$

$$\langle \cos^2\theta_{i/2} \rangle = 1 - \langle \cos^2\theta_{i/1} \rangle \quad (4)$$

$$\langle \cos^4\theta_{i/3} \rangle = 0 \quad (5)$$

$$\langle \cos^4\theta_{i/2} \rangle = 1 - 2\langle \cos^2\theta_{i/1} \rangle + \langle \cos^4\theta_{i/1} \rangle \quad (6)$$

Therefore, up to the fourth order, there are only two independent moments, $\langle \cos^2\theta_{i/1} \rangle$ and $\langle \cos^4\theta_{i/1} \rangle$ for instance. To simplify the notation, let us call $C_2 = \langle \cos^2\theta_{i/1} \rangle$, $C_4 = \langle \cos^4\theta_{i/1} \rangle$ and $\theta_{i/1} = \theta$.

Physical meaning of C_2. In the special case where all units have their axes oriented preferentially along the X_1 or X_2 axes, C_2 gives very useful and simple information about the distribution. Let us first model the planar distribution by the sum of two Gaussian distributions, one centred along X_1, the other one along X_2. The total

distribution can be written:

$$N(\theta) = N_1 \exp\left(-\ln 2\left(\frac{\theta}{\delta\theta_1}\right)^2\right) + N_2 \exp\left(-\ln 2\left(\frac{\pi/2-\theta}{\delta\theta_2}\right)^2\right) \quad (7)$$

where $\delta\theta_1$ and $\delta\theta_2$ are the half-widths of the distributions centred along X_1 and X_2, respectively.

The fraction of units belonging to the family preferentially oriented along X_1 is given by

$$\frac{\int_{0°}^{90°} N_1 \exp\left(-\ln 2\left(\frac{\theta}{\delta\theta_1}\right)^2\right) d\theta}{\int_{0°}^{90°} N(\theta)\, d\theta} \quad (8)$$

and C_2 is calculated as

$$C_2 = \frac{\int_{0°}^{90°} N(\theta)\cos^2\theta\, d\theta}{\int_{0°}^{90°} N(\theta)\, d\theta} \quad (9)$$

In *Figure 1*, C_2 is plotted *versus* the fraction of axis oriented along X_1 for different values of half-width $\delta\theta = \delta\theta_1 = \delta\theta_2$. Even when distributions overlap, for a given half-width, there is a linear relationship between C_2 and the fraction of units oriented along X_1. The relationship is, however, not unequivocal and the description of the distribution requires the use of C_4. The calculation of the most probable distribution function is then useful to provide a representation of the distribution function from experimental data.

Most probable distribution. In the case of a distribution restricted in a plane for which C_2 and C_4 are known, the MPDF can be expressed as

$$\mathrm{MPDF}(\theta) = A\exp(a_2\cos^2\theta + a_4\cos^4\theta) \quad (10)$$

where A is a normalization constant and the coefficients a_2 and a_4 are such that

$$C_2 = \frac{\int \mathrm{MPDF}(\theta)\cos^2\theta\, d\theta}{\int \mathrm{MPDF}(\theta)\, d\theta} \quad (11)$$

$$C_4 = \frac{\int \mathrm{MPDF}(\theta)\cos^4\theta\, d\theta}{\int \mathrm{MPDF}(\theta)\, d\theta} \quad (12)$$

Depending on the respective value of a_2 and a_4, three kinds of limiting distributions can be constructed:

(i) a monodistribution centered along X_1 or X_2;
(ii) a bidistribution where the units are preferentially aligned along X_1 or X_2;
(iii) an eccentered monodistribution having its maximum at an intermediate angle between X_1 and X_2.

Polarized fluorescence for a biaxial system

Application of fluorescence polarization to the measurement of molecular orientation is based on the

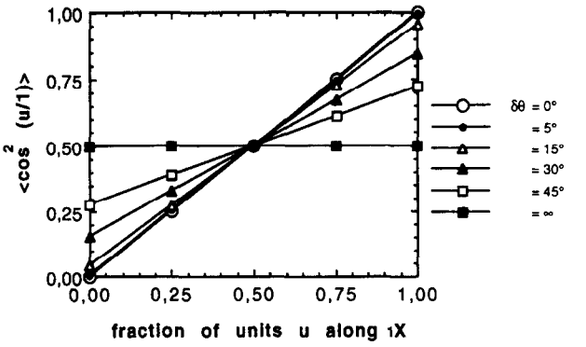

Figure 1 C_2 *versus* the fraction of units belonging to the Gaussian family along X_1 for different half-widths $\delta\theta = \delta\theta_1 = \delta\theta_2$

orientation of the transition moment, in both absorption and emission, of a fluorescent molecule with respect to the principal directions of the sample. The fluorescent intensity $I(P, A)$ measured when the polarizer and the analyser are set in the direction P and A, respectively, is given by[15,23]

$$I(P, A) = K\langle\cos^2(P, M_a)\cos^2(A, M_e)\rangle \quad (13)$$

where M_a and M_e are the directions of the transition moments in absorption and emission, respectively, the brackets meaning an average over all the fluorescent molecules.

In the case of rigid media, for which the fluorescent molecule does not undergo any motion during the lifetime of the excited state, the measurement of six independent fluorescence intensities yields five averages of Legendre polynomials in the general case of biaxial symmetry[3]. Corrections have to be applied to take into account the so-called fundamental anisotropy of the probe r_0 (ref. 3).

The quantity r_0, which can be obtained from the depolarization of an isotropic sample, is related to the delocalization of the transition moments in absorption and emission with respect to an average molecular direction M of the fluorescent molecule. It is usually admitted that the delocalization is the same in absorption and emission, so that $a = P_{200}^{M_a/M} = P_{200}^{M_e/M} = (5r_0/2)^{1/2}$.

An experimental method has been described previously to obtain five intensity ratios in order to characterize the orientation in biaxially oriented materials[3]. It has been successfully checked and applied in the case of one-way drawn films (uniaxial/planar symmetry). For the samples investigated in this study, this method led to unrealistic results, mainly due to the fact that fluorescent probes almost lie in the plane of the film. In this case, some intensities become very weak and are strongly affected by the film flatness. In order to overcome this difficulty, we will assume that the probes lie in the plane of the film, so that the measurement of only two intensity ratios is required to characterize the second and fourth order moments of the orientation distribution function of the probes. The derivation of the probe orientation from the measured intensities is given in the Appendix, taking into account the delocalization effects.

Conventions

In the case of biaxial stretching, the macroscopic directions are the principal directions of the film. They

will be referred to as machine direction (MD) for the direction of the first longitudinal stretching (OX_1), transverse direction (TD) for the direction of the second transverse drawing (OX_2), and normal direction (ND) for the direction normal to the plane of the film (OX_3).

EXPERIMENTAL

Fluorescence polarization

It has been shown by several authors[24,27] that a fluorescent probe like the VPBO inserted within a polymer matrix has a tendency to orient its long axis M along the polymer chain axis during stretching. Since the probe is rejected from the crystalline phase of the polymer, it provides specific information about the orientation of the polymer chain axes belonging to the amorphous phase. More precisely, in the case of a VPBO probe inserted within a PET matrix, Nobbs *et al.*[26] showed that the long axis of the probe tends to reflect the orientation of *trans* sequences in the amorphous phase rather than the average amorphous orientation.

We have used the experimental set-up in reflection described by Lapersonne *et al.*[3]. It allows us to measure four intensity ratios:

$$\frac{I_{11}}{I_{12}}, \frac{I_{22}}{I_{12}}, \frac{I_{13}}{I_{12}}, \frac{I_{23}}{I_{12}}$$

where I_{ij} designs the fluorescence intensity measured with the excitation beam polarized along direction i and the emitted one polarized along direction j.

In our case, experimental determination of these first four ratios leads to the conclusion that

$$\frac{I_{11}}{I_{12}}, \frac{I_{22}}{I_{12}} \gg \frac{I_{13}}{I_{12}}, \frac{I_{23}}{I_{12}} \tag{14}$$

It seems, therefore, a reasonable approximation to consider that all the fluorescent probes have their M axes in the plane of the film, the non-zero intensities measured out of the plane of the film being only due to the delocalization of the moments of absorption and emission. This hypothesis is compatible with results previously obtained by Lapersonne *et al.* for one-way drawn PET films. As an illustration, values of $\langle\cos^2(M,X_i)\rangle$ and $\langle\cos^4(M,X_i)\rangle$ of one-way drawn films at different draw ratios obtained by Lapersonne *et al.*[3] are reported in *Table 2*. It appears clearly that, at the end of the first drawing, $\langle\cos^2(M,X_3)\rangle$ and $\langle\cos^4(M,X_3)\rangle$ are very weak. Taking into account the symmetry of the deformation tensor in the transverse stretching, even weaker values are expected in the final films.

Table 2 Second and fourth order moments of one-way drawn films

	$\langle\cos^2 M,x_i\rangle$			$\langle\cos^4 M,x_i\rangle$		
λ_1	X_1	X_2	X_3	X_1	X_2	X_3
3,0	0.72_0	0.19_5	0.10_6	0.62_7	0.10_2	0.09_9
3,2	0.74_7	0.18_9	0.08_6	0.65_5	0.09_7	0.08_7
3,4	0.81_2	0.16_3	0.03_9	0.73_9	0.09_0	0.05_9
3,6	0.92_6	0.12_6	-0.02_9	0.85_7	0.05_7	0.00_6

Refractive indices

The refractive indices of the samples were measured along the three principal directions using an Abbe refractometer under polarized light.

Density d and crystallinity χ were calculated from the mean refractive index $\bar{n} = n_1 + n_2 + n_3/3$ by the following formulae[28].

$$d = 4.047\left(\frac{\bar{n}^2 - 1}{\bar{n}^2 + 2}\right) \tag{15}$$

$$\chi = \frac{d - d_a}{d_c - d_a} \tag{16}$$

where d_a is the density of the amorphous phase and d_c is the density of the crystalline phase. These were taken to be 1.335 and 1.455 g cm^{-3}, respectively[29].

Overall orientation of the normal to the phenyl ring

If $Ox_1x_2x_3$ is an orthogonal set of axes attached to the molecular unit of the PET chain, where Ox_1 is parallel to the chain axis, Ox_2 is perpendicular to Ox_1 and in the plane of the ring, and Ox_3 will be close to the normal to the ring. If α_i is the molecular polarizability along i, it has been shown[8] that within a good approximation, the following relationship holds:

$$P_{200}^{n/I} = P_{200}^{3/I} = \frac{1}{\Delta}\frac{\phi_I - (\phi_J + \phi_K)/2}{\phi_I + \phi_J + \phi_K} \tag{17}$$

where

$$\Delta = \frac{\alpha_3 - (\alpha_1 + \alpha_2)/2}{\alpha_1 + \alpha_2 + \alpha_3} \text{ and } \phi_I = \frac{n_I^2 - 1}{n_I^2 + 2}$$

where I, J and K refers to the MD, TD and ND directions.

Overall orientation of the chain axis

It is possible to obtain the second order Legendre moment of the chain axis $P_{200}^{c/I}$ averaged over all the material with respect to any direction I of the film from i.r. spectroscopy measurements. *Figure 2* shows the orientation of the normal to the ring with respect to X_1 (and X_2) measured by refractive indices plotted *versus* the orientation of the chain axes measured by i.r. spectroscopy with respect to the same directions for samples characterized by both techniques[8]. On the same figure are reported the data of Lapersonne *et al.*[7] for

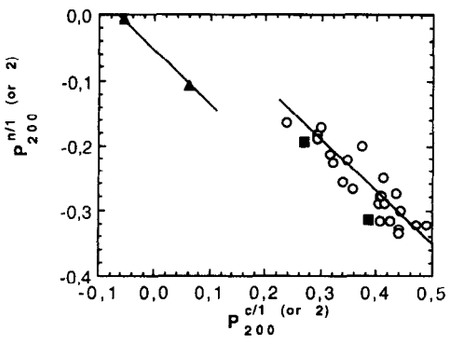

Figure 2 $P_{200}^{n/I}$ *versus* $P_{200}^{c/I}$ for (○) one-way drawn samples [$I = 1$ (machine direction)]; (■) transversally drawn samples [$I = 2$ (transverse direction)]; (▲) transversally drawn samples ($I = 1$ (machine direction)]

one-way drawn films. The chain axis orientation appears to be correlated with the orientation of the phenyl ring's normal for uniaxial planar stretching: this is true for the first (longitudinal) stretching as well as for the second (transversal) stretching. This relationship between the orientation of the ring normals and the chain axes is of interest since it allows an estimate of the second order orientation moment of the chain axes from refractive indices data only. Because of thickness limitations, few sequentially drawn films have been studied by i.r. dichroism, generating some uncertainty for the relationship between the ring normal and the chain axis. Two separate regimes appear clearly in *Figure 2*; for high values of λ_2 ($\lambda_2 > 3$), the film behaves in the same way with respect to the X_2 axis (X_1) as it was behaving with respect to X_1 (X_2) at the end of the first drawing (when $\lambda_2 = 1$) and the following relationships hold:

$$P_{200}^{c/1} = -0.122 - 1.502\,P_{200}^{n/1} \tag{18a}$$

$$P_{200}^{c/2} = 0.096 - 1.079\,P_{200}^{n/2} \tag{18b}$$

Orientation in the amorphous phase

Knowing the orientation of the ring normal and the chain axis in the crystalline phase and on average in the material, it is possible to deduce the orientation of these molecular directions i with respect to the film directions J in the amorphous phase, assuming a two-phases model:

$$(P_{200}^{i/J})_{\text{amorphous}} = \frac{(P_{200}^{i/J})_{\text{average}} - \chi(P_{200}^{i/J})_{\text{cryst}}}{1-\chi} \tag{19}$$

In our case, the orientation of the $(\bar{1}\,0\,5)$ planes normals will be taken as the orientation of the chain axes in the crystalline phase and that given by the (1 0 0) reflection will be considered as that of the phenyl rings normals, although the crystallographic directions do not exactly coincide with the molecular ones.

EXPERIMENTAL RESULTS CONCERNING THE AMORPHOUS PHASE

In the following sections, the influence of the preheating stage can be appreciated by the differences between data points corresponding to $\lambda_2 = 0.5$ (before preheating) and to $\lambda_2 = 1$ (after preheating).

Orientation of the ring normal

The orientation moments $P_{200}^{n/I}$ of the ring normals in the amorphous phase with respect to the principal axes of the film have been calculated as explained in Experimental. Their evolution with the draw ratio is reported in *Figures 3a–c*. As expected, the level of orientation is lower in the amorphous phase than in the crystalline phase[9].

With respect to the first stretching direction X_1, the phenyl rings normal in the amorphous phase lose their perpendicularity as the draw ratio increases and this behaviour does not seem much affected by the crystalline morphology of the one-way drawn films. In the crystalline phase, it has been shown previously that the ring normals remain essentially perpendicular to X_1 throughout the second stretching.

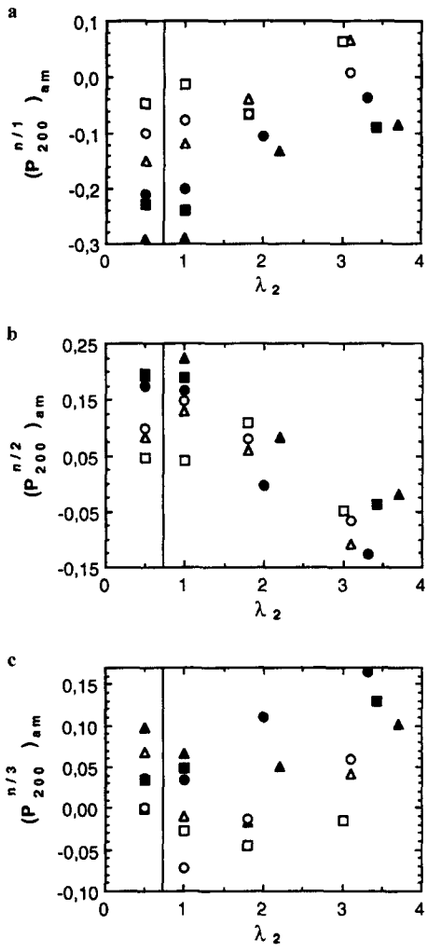

Figure 3 Orientation of the normal to the phenyl ring with respect to (a) the machine direction, (b) transverse direction and (c) normal direction *versus* draw ratio: (△) $s_{100,3.2}$; (□) $s_{103,3.4}$; (○) $s_{105,3.2}$; (▲) $l_{100,3.9}$; (■) $l_{105,3.6}$; (●) $l_{125,3.4}$

The increase in perpendicularity of the ring normals with respect to the second drawing axis X_2 is similar for films with initially short or long crystals, and the perpendicularity level is finally higher for films with initially short crystals (*Figure 3b*). This final situation is rather similar to that observed in the crystalline phase. However, in the crystalline phase, the variation of orientation was larger in films having initially short crystals.

The increase in orientation of ring normals with respect to the film normal X_3 during the second drawing is similar for films having initially short or long crystals. The orientation's level remains slightly higher for films with initially long crystals (*Figure 3c*). Whereas in the crystalline phase, phenyl rings tend to lie in the plane of the film, in the amorphous phase this tendency is not evidenced. During the second drawing, the increase in $P_{200}^{n/3}$ is close to the increase in $P_{200}^{n/1}$: the stretching along an X_i axis tends to increase the perpendicularity of the ring normal with respect to this axis X_i in a quasi-uniaxial way in the amorphous phase, although the deformation tensor is not uniaxial.

Orientation of the chain axis from refractive indices measurements

Since the chain axis orientation is calculated from the

same data as that for the phenyl ring's normal, the same tendencies are expected. It might, however, be easier to think in terms of the chain axis rather than of a perpendicular molecular direction.

The orientation moments $P_{200}^{c/I}$ of the chain axis in the amorphous phase have been calculated as explained above. Their evolution during transverse stretching is plotted in *Figures 4a–c*. In the crystalline phase[9], a strong loss of orientation was observed with respect to the first stretching direction X_1: a similar behaviour, although less pronounced, was observed for the amorphous phase (*Figure 4a*), the loss in perpendicularity being lower in the case of films with initially long crystals as observed in the crystalline phase.

In the amorphous phase (*Figure 4b*), a significant increase in chain axis orientation is observed with respect to the draw direction (almost of the same order of magnitude as in the crystalline phase). The influence of the size of the crystals is much weaker than observed in the crystalline phase. The highest difference between both phases is dealing with the chain axes orientation with respect to the normal direction. In the crystalline phase, chain axes are initially perpendicular to the film normal X_3 and remain in this state throughout the stretching. At the beginning of the second drawing, the perpendicularity of the chain axes with respect to X_3 is fairly low in the amorphous phase for films having initially short crystals and somewhat higher for films with initially long crystals (*Figure 4c*). During the second drawing, there is a large increase in perpendicularity with respect to X_3 whatever the initial size of the crystals in the amorphous phase. Chain axes in the amorphous phase show a tendency to orient in the plane of the film during the transverse drawing.

Table 3 Characteristics of sequentially drawn samples filled with VPBO probe

Original one-way drawn film	λ_2	$P_{200}^{M/1}$	C_2	C_4
$s_{100.3.2}$	1.0	0.69_4	0.79_6	0.69_8
	2.0	0.31_8	0.54_5	0.41_3
	3.0	-0.02_3	0.31_8	0.16_7
$s_{100.3.3}$	1.0	0.71_7	0.81_1	0.72_4
	1.9	0.40_5	0.60_3	0.46_8
	3.0	0.02_2	0.34_8	0.21_2
$s_{105.3.2}$	1.0	0.57_3	0.71_5	0.60_1
	1.6	0.37_9	0.58_6	0.45_8
	3.1	0.06_0	0.37_3	0.23_9
$s_{105.3.5}$	1.0	0.58_0	0.72_0	0.61_1
	1.7	0.32_7	0.55_1	0.42_9
	3.1	0.09_7	0.39_8	0.25_9
$l_{100.3.9}$	1.0	0.79_8	0.86_5	0.77_5
	1.9	0.67_9	0.78_6	0.69_2
	3.9	0.07_6	0.38_0	0.18_2
$l_{105.3.6}$	1.0	0.76_2	0.84_1	0.75_8
	3.4	0.25_2	0.50_1	0.28_4

Orientation of a VPBO probe from fluorescence spectroscopy

Table 3 lists the samples studied by fluorescence polarization and the corresponding values of $C_2 = \langle\cos^2(M, X_1)\rangle$, $C_4 = \langle\cos^4(M, X_1)\rangle$ and the second Legendre polynomial $P_{200}^{M/1}$, obtained under the assumption that all probe axes are in the plane of the film.

The $P_{200}^{M/1}$ values are almost positive whereas the chain axes in the crystalline phase for the same samples show negative values of this quantity. Thus, VPBO molecules show a lower tendency to orient along the transverse stretching axis X_2 as compared to the chain axes in the crystalline phase. The evolution of $P_{200}^{M/1}$ *versus* the draw ratio is reported in *Figure 5*. A strong difference in $P_{200}^{M/1}$ values between transversally drawn samples having initially short or long crystal can be noted. $P_{200}^{M/1}$ remains higher for samples having initially long crystals, indicating a less efficient reorientation of the probes towards the transverse direction as compared to the

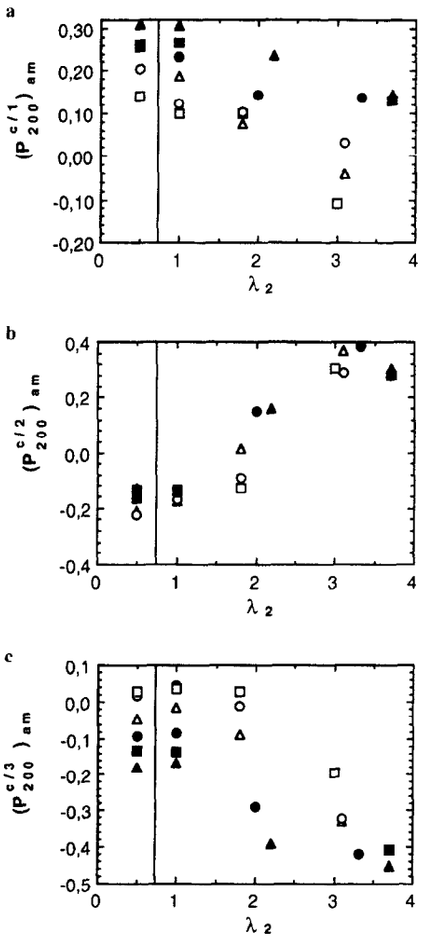

Figure 4 Orientation of the chain axes with respect to (a) the machine direction, (b) transverse direction and (c) normal direction *versus* draw ratio: (△) $s_{100,3.2}$; (□) $s_{103,3.4}$; (○) $s_{105,3.2}$; (▲) $l_{100,3.9}$; (■) $l_{105,3.6}$; (●) $l_{125.3.4}$

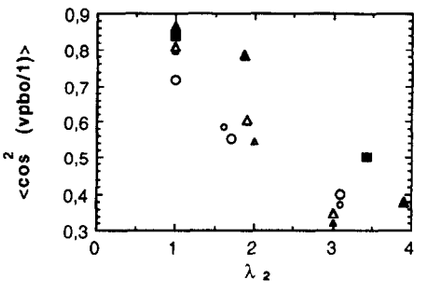

Figure 5 Orientation of the VPBO probe in the film plane: C_2 *versus* λ_2 with respect to the machine direction: (△) $s_{100,3.2}$; (△) $s_{100.3.3}$; (○) $s_{105.3.2}$; (○) $s_{105,3.5}$; (▲) $l_{100.3.9}$; (■) $l_{105.3.6}$

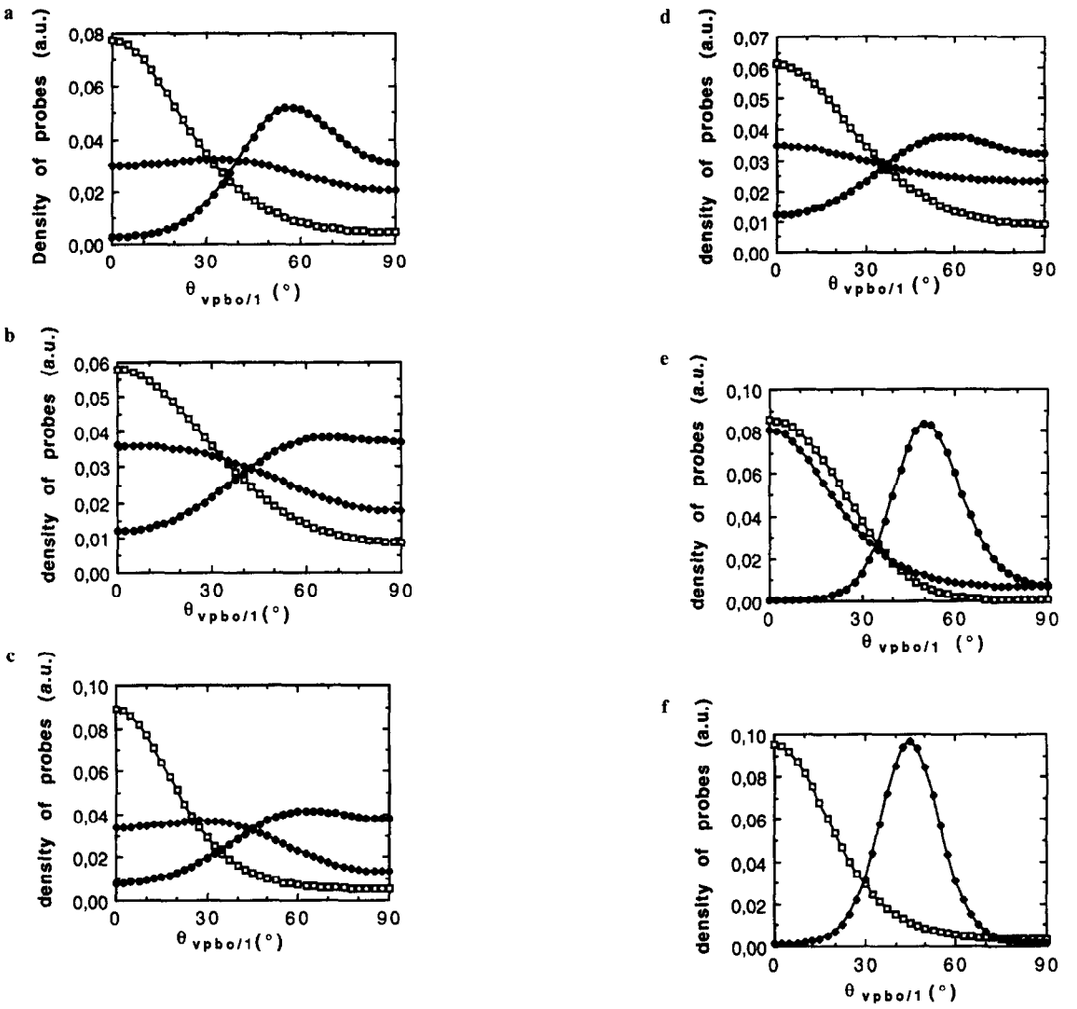

Figure 6 Most probable distributions obtained for (a) (□) $s_{100,3.2/120,1.0}$, (◆) $s_{100,3.2/120,1.7}$ and (●) $s_{100,3.2/120,3.1}$; (b) (□) $s_{105,3.2/120,1.0}$, (◆) $s_{105,3.2/120,1.7}$ and (●) $s_{105,3.2/120,3.1}$; (c) (□) $s_{100,3.3/120,1.0}$, (◆) $s_{100,3.3/120,1.9}$ and (●) $s_{100,3.3/120,3.0}$; (d) (□) $s_{105,3.5/120,1.0}$, (◆) $s_{105,3.5/120,1.7}$ and (●) $s_{105,3.5/120.3.1}$; (e) (□) $l_{100,3.9/120,1.0}$, (◆) $l_{100,3.9/120,1.6}$ and (●) $l_{100,3.9/120,3.8}$; (f) (□) $l_{105,3.6/120,1.0}$ and (◆) $l_{105,3.6/120,3.7}$

other type of films; the same trends were observed for the chain axes in the amorphous phase.

Films having short crystals at the end of the first drawing were obtained at different temperatures. Those stretched at $T_1 = 100°C$ (during the first draw), although being initially more oriented, loose their orientation faster with respect to X_1 than the one stretched at $T_1 = 105°C$. This behaviour is similar to that observed for chain axes orientation deduced from refractive indices measurements.

This can be explained by the fact that higher stretching temperatures lead to a more rapid relaxation of the amorphous phase during the first drawing and therefore a loss in orientation of the chain axes; the VPBO probe orientation is then lower. Moreover, low temperatures lead to smaller crystals. The destruction of the crystalline structure oriented along the X_1 direction is easier and this favours the rotation of the probe axes towards the new stretching direction X_2. The increase in orientation of the probe axes with respect to X_2 is then higher for films drawn at lower temperature during the first drawing.

More detailed information can be obtained if the C_4 values measured by fluorescence polarization are taken into account. As a visual aid, the most probable orientation distributions of the probe axes were calculated. *Figure 6* shows the most probable distribution for each sample and the various second draw ratios. The distributions are drawn such that the total number of probes is the same in all the figures. As deformation proceeds, the probe axes distributions become larger and a rotation of a large part of the probes is observed. This behaviour, already apparent in films with initially small crystals, is clearly shown in the case of films having initially long crystals. However, in the former case, the distribution becomes fairly isotropic at intermediate λ_2 and becomes sharper again when the film is further transversally stretched. This behaviour is not observed in films having initially long crystals. No bidistribution is observed in the amorphous phase although the bidistribution of chain axes in the crystalline phase is one of the main features of the second stretching. A more detailed analysis of the most probable distribution curves show that a memory of the broadness of the distribution is kept during the second stretching. For instance, sample s_{105} shows at $\lambda_2 = 1$ a broader distribution than sample s_{100}. This is still the case at the end of the second drawing ($\lambda_2 = 3.1$). The same remark is valid if samples l_{100} and l_{105} are compared.

The most striking feature of these fluorescence data is the appearance of eccentred maxima in the most probable distribution, especially in sample containing large crystals. It seems to imply a rotation as a whole during the transverse stretching of the probes that are machine oriented at the end of the first drawing process. Analysis of literature dealing with intrinsic fluoresence polarization data for uniaxially drawn films shows that the maximum of the orientation distribution function tends to deviate from the stretching direction at large extensions[30,31]. It is at present not clear to decide whether this physically strange behaviour results from experimental artefacts arising at large extensions (changes of the polarization due to some light scattering) or implies a deformation mechanism different from the affine or pseudo-affine ones[32]. However, comparison of crystallinities and the final sizes of crystals in our various samples shows that they are quite similar, whereas large differences are seen by fluorescence polarization.

CONCLUSION

This study of amorphous phase orientation, deduced by assuming a two-phase model or from the behaviour of rigid fluorescent probes, affords new information on the molecular behaviours during stretching. It is first shown that the phenyl rings in the amorphous phase do not tend to lie preferentially in the plane of the film, contrary to the behaviour known for the crystalline phase. During the second drawing, the rotation of chain axes in the amorphous phase towards the second drawing direction X_2 is more difficult for films having long crystals at the end of the first stretching. The same phenomenon is observed for VPBO probes: for a draw ratio of 1.9, the maximum of the probe distribution remains along the first stretching direction; at such a draw ratio, this means that the probes axes are slightly rotating, but are also moving parallel one to each other and to the first drawing direction X_1. The behaviour of the VPBO probes is fairly different for films having initially short crystals; in this case, the distribution of probe axes are much more isotropic in the film plane. There seems to be a rotation of these probe axes following the material deformation according qualitatively to a pseudo-affine model.

AKNOWLEDGEMENT

The authors are grateful to Rhône Poulenc Films for providing a Ph.D. Fellowship to one of us (J. B. F.).

REFERENCES

1. Le Bourvellec, G., Monnerie, L. and Jarry, J. P., *Polymer*, 1986, **27,** 855.
2. Le Bourvellec, G., Monnerie, L. and Jarry, J. P., *Polymer*, 1987, **28,** 1712.
3. Lapersonne, P., Tassin, J. F., Sergot, P., Monnerie, L. and Le Bourvellec, G., *Polymer*, 1989, **30,** 1558.
4. Lapersonne, P., Tassin, J. F., Monnerie, L. and Beautemps, J., *Polymer*, 1991, **32,** 3331.
5. Lapersonne, P., Bower, D. I. and Ward, I. M., *Polymer*, 1992, **33,** 1266.
6. Lapersonne, P., Bower, D. I. and Ward, I. M., *Polymer*, 1992, **33,** 1277.
7. Lapersonne, P., Tassin, J. F. and Monnerie, L., *Polymer*, 1994, **35,** 2192.
8. Faisant de Champchesnel, J. B., Bower, D. I., Ward, I. M., Tassin, J. F. and Lorentz, G., *Polymer*, 1993, **34,** 3763.
9. Faisant de Champchesnel, J. B., Bower, D. I., Ward, I. M., Tassin, J. F. and Lorentz, G., *Polymer*, 1994, **35,** 4092.
10. Stein, R. S. and Norris, F. H., *J. Polym. Sci.*, 1956, **21,** 381.
11. Moseley, W. W., *J. Appl. Polym. Sci.*, 1960, **3,** 226.
12. Samuels, R. J., *J. Polym. Sci. A*, 1965, **3,** 1741.
13. Henrichs, P. M., *Macromolecules*, 1987, **20,** 2099.
14. Chemlka, B. F., Schmidt Rohr, K. and Spiess, H. W., *Macromolecules*, 1993, **26,** 2282.
15. Ward, I. M., *Adv Polym. Sci.*, 1985, **66,** 81.
16. Hennecke, M. and Fuhrmann, J., *Makromol. Symp.*, 1986, **5,** 181.
17. Hemker, D. J., Franck, C. W. and Thomas, J. W., *Polymer*, 1988, **29,** 437.
18. Clauss, B. and Salem, D. R., *Polymer*, 1992, **15,** 3193.
19. Lebourvellec, G., Jarry, J. P. and Beautemps, J., *J. Appl. Polym. Sci.*, 1990, **39,** 319.
20. Lebourvellec, G. and Beautemps, J., *J. Appl. Polym. Sci.*, 1990, **39,** 329.
21. Bower, D. I., *J. Polym. Sci.: Polym. Phys. Edn*, 1981, **19,** 93.
22. Bower, D. I., *Polymer*, 1982, **23,** 1251.
23. Monnerie, L. in *Static and Dynamic Properties of the Polymeric Solid State*, ed. R. A. Pethrick and R. W. Richards. Reidel, London, 1981, p. 383.
24. Nobbs, J. H., Bower, D. I., Ward, I. M. and Patterson, D. P., *Polymer*, 1974, **15,** 287.
25. Nobbs, J. H., Bower, D. I., Ward, I. M. and Patterson, D. P., *Polymer*, 1976, **17,** 25.
26. Nobbs, J. H., Bower, D. I. and Ward, I. M., *J. Polym. Sci.: Polym. Phys. Edn.*, 1979, **17,** 259.
27. Bower, D. I., Korybut-Daskiewicz, K. K. P. and Ward, I. M., *J. Appl. Polym. Sci.*, 1983, **28,** 1195.
28. De Vries, A. J., Bonnebat, C. and Beautemps, J., *J. Polym. Sci.*, 1977, **58,** 109.
29. Daubeny, R., Bunn, C. W. and Brown, C. J., *Proc. Roy. Soc., London*, 1954, **226,** 531.
30. Hennecke, M., Kud, A., Kurz, K. and Fuhrmann, J., *J. Colloid Polym. Sci.*, 1987, **265,** 764.
31. Hennecke, M., Kurz, K. and Fuhrmann, J. *Macromolecules*, 1992, **25,** 6190.
32. Ward, I. M., *Structure and Properties of Oriented Polymers*. Applied Science, London, 1975.

APPENDIX

Following the formalism given in ref. 3, the six measured fluorescence intensities I_{ij} are related to orientation coefficients $C_{ij}(=\langle\cos^2(M,X_i).\cos^2(M,X_j)\rangle)$ by the following relationships:

$$I_{11} = \left(\frac{a}{3}+\frac{2a^2}{3}\right)C_{11} + \left(\frac{a}{3}-\frac{a^2}{3}\right)(-C_{22}-C_{33}-2C_{23}) + \frac{1+a-2a^2}{9} \quad \text{(A1)}$$

$$I_{22} = \left(\frac{a}{3}+\frac{2a^2}{3}\right)C_{22} + \left(\frac{a}{3}-\frac{a^2}{3}\right)(-C_{11}-C_{33}-2C_{13}) + \frac{1+a-2a^2}{9} \quad \text{(A2)}$$

$$I_{33} = \left(\frac{2a}{3}+\frac{a^2}{3}\right)C_{33} + \left(\frac{2a}{3}-\frac{2a^2}{3}\right)(C_{13}+C_{23}) + \frac{1+2a-2a^2}{9} \quad \text{(A3)}$$

$$I_{23} = \left(\frac{2a}{3} + \frac{a^2}{3}\right) C_{33} + \left(\frac{2a}{3} - \frac{2a^2}{3}\right)(C_{13} + C_{23}) + \frac{1 - 2a + a^2}{9} \quad \text{(A4)}$$

$$I_{13} = \left(\frac{a}{3} + \frac{2a^2}{3}\right) C_{13} + \left(\frac{a}{6} - \frac{a^2}{6}\right)(C_{11} - C_{22} + C_{33}) + \frac{2 - a - a^2}{18} \quad \text{(A5)}$$

$$I_{23} = \left(\frac{a}{3} + \frac{2a^2}{3}\right) C_{23} + \left(\frac{a}{6} - \frac{a^2}{6}\right)(-C_{11} + C_{22} + C_{33}) + \frac{2 - a - 2a^2}{18} \quad \text{(A6)}$$

When the moments of absorption M_a and emission M_e are lying along the axis M of the probe, then $a = 1$, and we find $I_{ij} = C_{ij}$ whatever i or j, as expected. When those moments do not show any peculiar orientation with respect to M, then $a = 0$: this is the case when fluoresence is totally depolarized; we then find $I_{ij} = 1/9$ whatever i or j, as expected.

In the special case where the M axes of all the probes are contained in a plane (let us take $X_1 0 X_2$ to be this plane), the only orientation coefficients which are different from 0 are: C_{11}, C_{22}, C_{12} and C_{21}. The above (A1–A6) relationships then reduce to

$$C_{11} = \frac{\frac{(2a+1)^2}{9a^2} r_1 + \frac{(a-1)^2}{9a^2} r_2 + \frac{2(2a+1)(a-1)}{9a^2}}{r_1 + r_2 + 2} \quad \text{(A7)}$$

$$C_{22} = \frac{\frac{(a-1)^2}{9a^2} r_1 + \frac{(2a+1)^2}{9a^2} r_2 + \frac{2(2a+1)(a-1)}{9a^2}}{r_1 + r_2 + 2} \quad \text{(A8)}$$

$$C_{12} = \frac{1 - C_{11} - C_{22}}{2} \quad \text{(A9)}$$

with

$$r_1 = \frac{I_{11}}{I_{12}} \text{ and } r_2 = \frac{I_{22}}{I_{12}} \quad \text{(A10)}$$

It is then possible to obtain the value of the second and fourth order moments of M with respect to the reference axes X_1, X_2 and X_3:

$$\langle \cos^2(M, X_1) \rangle = C_{11} + C_{12} \quad \text{(A11)}$$

$$\langle \cos^2(M, X_2) \rangle = C_{12} + C_{22} \quad \text{(A12)}$$

$$\langle \cos^2(M, X_3) \rangle = 0 \quad \text{(A13)}$$

$$\langle \cos^4(M, X_1) \rangle = C_{11} \quad \text{(A14)}$$

$$\langle \cos^4(M, X_2) \rangle = C_{22} \quad \text{(A15)}$$

$$\langle \cos^4(M, X_3) \rangle = 0 \quad \text{(A16)}$$